Biosensors and Bioelectronics 189 (2021) 113307

Contents lists available at ScienceDirect

Biosensors and Bioelectronics

journal homepage: www.elsevier.com/locate/bios

Electrophoretic mobility shift as a molecular beacon-based readout for miRNA detection

Getulio P. Oliveira-Jr [a,*], Raquel H. Barbosa [a], Lauren Thompson [b], Brandy Pinckney [b], Moriah Murphy-Thornley [a], Shulin Lu [a], Jennifer Jones [c], Clinton H. Hansen [d], John Tigges [b], Wesley P. Wong [d], Ionita C. Ghiran [a,**]

[a] Division of Allergy and Inflammation, Department of Medicine, Beth Israel Deaconess Medical Center, Harvard Medical School, Boston, MA, United States
[b] Nano Flow Core Facility, Beth Israel Deaconess Medical Center, Harvard Medical School, Boston, MA, United States
[c] Laboratory of Pathology Center for Cancer Research, National Cancer Institute, Bethesda, MD, United States
[d] Program in Cellular and Molecular Medicine, Boston Children's Hospital, Department of Biological Chemistry and Molecular Pharmacology, Blavatnik Institute, Harvard Medical School, Wyss Institute for Biologically Inspired Engineering, Harvard University, Boston, MA 02115, USA

ARTICLE INFO

Keywords:
Molecular beacons
Electrophoretic mobility
Gel electrophoresis
microRNA (miRNA)

ABSTRACT

MicroRNAs are short, non-coding RNA sequences involved in gene expression regulation. Quantification of miRNAs in biological fluids involves time consuming and laborious methods such as Northern blotting or PCR-based techniques. Molecular beacons (MB) are an attractive means for rapid detection of miRNAs, although the need for sophisticated readout methods limits their use in research and clinical settings. Here, we introduce a novel method based on delayed electrophoretic mobility, as a quantitative means for detection of miRNAs-MB hybridization. Upon hybridization with the target miRNAs, MB form a fluorescent duplex with reduced electrophoretic mobility, thus bypassing the need for additional staining. In addition to emission of light, the location of the fluorescent band on the gel acts as an orthogonal validation of the target identity, further confirming the specificity of binding. The limit of detection of this approach is approximately 100 pM, depending on the MB sequence. The method is sensitive enough to detect specific red blood cell miRNAs molecules in total RNA, with single nucleotide specificity. Altogether, we describe a rapid and affordable method that offers sensitive detection of single-stranded small DNA and RNA sequences.

1. Introduction

Molecular beacons (MB) are hairpin-shaped oligonucleotides (RNA or DNA) that contain an anti-sense hybridization sequence matched to a specific single-stranded RNA or DNA molecule, a double-stranded stem region, and at its termini, a fluorochrome and a quencher (Tyagi and Kramer, 1996). In the absence of the target, the stem sequence keeps the quencher and the fluorochrome into close proximity preventing the MB from fluorescing. Binding of the MB to the target by the hybridization sequence triggers a conformational change in the stem which opens the beacon and separates the quencher from the fluorochrome, allowing emission of fluorescence upon excitation (Tan et al., 2004). Only the binding of the MB with the intended ssRNA or ssDNA target should generate a fluorescence signal, although separation of the quencher from the fluorochrome by contaminating RNAses, or temperature-dependent changes in conformation could also have the same results (Burris et al., 2013). Using locked nucleic acids (LNA) instead of standard nucleotides when synthesizing the MBs can successfully alleviate this problem (Zhang et al., 2019). The readouts for the MB-generated signal classically involve fluorometry (Kam et al., 2012), microscopy (Chen et al., 2017), capillary electrophoresis (Li et al., 2011), flow cytometry (Horejsh et al., 2005) or nano-flow cytometry (de Oliveira et al., 2020).

MicroRNA molecules (miRNAs) were first described in the nematode *Caenorhabditis elegans* in early 1990 (Lee et al., 1993). These molecules are short, non-coding RNA sequences (19–22 nt) that primarily function as silencers of RNA expression, and regulators of gene expression (Bushati and Cohen, 2007). The array of functions of the miRNA-regulated RNA molecules is significant, spanning cell division (Hatfield et al., 2005), growth (Shi et al., 2016), differentiation (Wu

* Corresponding author.
** Corresponding author.
E-mail addresses: gpereira@bidmc.harvard.edu, junior.getulio@gmail.com (G.P. Oliveira-Jr), ighiran@bidmc.harvard.edu (I.C. Ghiran).

https://doi.org/10.1016/j.bios.2021.113307
Received 18 February 2021; Received in revised form 27 April 2021; Accepted 3 May 2021
Available online 15 May 2021

et al., 2018a), apoptosis (Li et al., 2018), and migration (Sandbothe et al., 2017). The number of confirmed mature miRNAs continues to increase, with their number to date of 1917 precursors, and 2654 mature for *Homo sapiens* [GRCh38](Kozomara et al., 2019). More recently, miRNAs have received increased attention for basic biological processes, and as biomarkers in liquid biopsy for disease diagnostics, progression, treatment efficacy and relapse (Izzotti et al., 2016). Quantitative detection of miRNAs in various biological fluids is usually performed using Northern blotting (Choi et al., 2017) or PCR-based techniques (Mestdagh et al., 2009), which are usually laborious and time consuming. More recently, MBs have started to be used successfully not only for the detection of, but also for the differentiation between miRNAs and pre-miRNAs (the loop sequence) using fluorometry as a readout method (James et al., 2017). Our group has used MBs coupled to cell penetrating peptides (CPP) for detection of miRNAs species in both cells and extracellular vesicles using super resolution microscopy and nano flow cytometry (de Oliveira et al., 2020). However, the cost of the CPP-MBs and of the necessary microscopes or flow cytometers for detection limits its use in point-of-care settings.

Additionally, we have recently developed molecular probes based on DNA self-assembly that we call DNA nanoswitches (Koussa et al., 2015). These structures consist of a long ssDNA scaffold almost 8000 bps long that has been titled with complementary oligonucleotides and decorated with affinity reagents that can bind to change the topology of the nanoswitch. These changes in topology can be read out using gel electrophoresis due to their effect on electrophoretic mobility. We have demonstrated high-sensitivity, high-specificity detection of protein biomarkers in serum by decorating each nanoswitch with a pair of sandwiching antibodies, in point-of-care (POC) settings (Hansen et al., 2017). Furthermore, by replacing the antibodies with strands of ssDNA complementary to nucleic acid sequences of interest, this concept has been extended to enable the detection of miRNAs(Chandrasekaran et al., 2019).

Herein, we report an electrophoretic-based method, complementary to the nanoswitches, which identifies the detection of specific ssRNA and ssDNA molecules by the coincident output of both delayed electrophoretic mobility and emission of fluorescence. Our approach does not require any staining, as the signal is provided by the fluorescence of the MB following the binding to the target ssRNA or ssDNA. Moreover, as the two means of detection are orthogonal (emission of fluorescence and changes in the electrophoretic speed of the single MB compared to the MB-target complex), this adds an additional level of specificity to the method. As our approach is straightforward, with no required washing or amplification steps, it can be used as a sensitive and easy-to-use assay in a laboratory setting or at the point-of-care.

2. Materials and methods

2.1. Reagents

Dulbecco's phosphate-buffered saline (dPBS, 2.6 mMKCl, 1.47 mM KH_2PO_4, 137 mMNaCl, and 8.05 mM Na_2HPO_4), Hanks' Balanced Salt Solution (HBSS–, no calcium, no magnesium, referred as HBSS) were obtained from Thermo Fisher Scientific (Waltham, MA). Invitrogen Novex™ TBE-Urea Gels, 15%, 10 well, and TBE-Urea Sample Buffer (2×), for denaturing conditions, and Novex™ TBE Running Buffer (5×), and Novex TBE Gels, 4–20% (non-denaturing conditions) were obtained from Thermo Fisher Scientific. Gel Loading Dye, purple (6×), without SDS was obtained from New England Biolabs (Ipswich, Massachusetts). Five hundred nanometer streptavidin beads were purchased from Bangs Laboratories (Fishers, IN). MiRCURY LNA miRNA Inhibitors (antimiRs) were obtained from Qiagen (Germantown, MD).

2.2. Molecular beacons and targets sequences

Molecular beacons and synthetic miRNAs or DNA oligonucleotide target analogs were obtained from Integrated DNA technologies IDT (Coralville, IA). All MBs were conjugated with a 5′ end 6-carboxyfluorescein (λ_{Ex} 495 nm; λ_{Em} 517 nm), and at the 3' end an internal ZEN quencher, followed by an 18-atom hexa-ethyleneglycol spacer (ISp18), and a biotin. The MBs were synthesized with the optimized stem sequence CGCGATC, as previously reported (Ryazantsev et al., 2014). The mutated miRNAs had the following modifications: M1, mutation from C to A in the 10th position; M2, mutation from CC to AA in the 10th and 11th positions; M3, mutation from U to C in the 22nd position (M3); and M4, mutation from UU to CC in the 21st and 22nd position. All the MBs and corresponding target sequences used for this project are shown in Table 1.

2.3. miRNA-MB hybridization detection by fluorometry

MBs were diluted in 100 μL of dPBS1X to a final concentration of 50 nM, and then incubated with different concentrations of synthetic miRNA oligonucleotide target analog (from 0 to 50 nM) in 96 well plates (Corning™ 96-Well clear bottom, black walls) for 30 min at 37 °C or 55 °C. The fluorescence intensity of each well was measured (λ_{Ex} 495 nm; λ_{Em} 521 nm) by a microplate reader (Synergy HT Multi-Mode, Biotek, Winooski, VT, USA). For the kinetics assay, MBs were diluted in 100 μL of dPBS1X to a final concentration of 50 nM, and then incubated with either 0, 50 nM target analog or 50 nM mismatch sequences in 96 well plates. Fluorescence (λ_{Ex} 495 nm; λ_{Em} 521 nm) was acquired at 55 °C every 5 min using a BioTek Synergy 4 fluorometer.

2.4. Coupling MB to streptavidin beads

Five hundred nm streptavidin beads were diluted in dPBS to a working concentration of 10,000 beads/uL (1:1000 dilution). Prior to conjugation to beads, 100 μM MBs were heated at 90 °C for 10 min, followed by centrifugation at 12,000×*g* for 20 min, as per manufacturer instructions. One microliter of the supernatant was added to 1 mL of 500 nm streptavidin beads and incubated at 37 °C for 15 min. After incubation, the MB-conjugated beads were washed once at 20,000×*g* for 10 min to remove any unbound MBs. MB-beads conjugates were then resuspended to a final volume of 200 uL.

2.5. miRNA-MB hybridization detection by flow cytometry

As the size of the streptavidin beads was 500 nm, the CytoFLEX LX flow cytometer was set up in the "nanoparticle detection mode" as previously reported (Camacho et al., 2017). Briefly, within the violet pod, the 450/45 bandpass was placed in position one and the 405/10 bandpass was placed in position two (Detector One). VSSC was used as the trigger parameter, and VSSCA linear versus SSCA log was plotted for bead population determination. The settings were optimized using Polysciences NIST Nanoparticle bead mix with sizes ranging from 80 to 500 nm, and set as follows: SSC: 58 V, VSSC: 50 V, FITC: 95 V, the FITC channel was used to measure the fluorescein fluorescence of the bead-attached MBs. For consistency, 50,000 events in the 500 nm gate population were recorded for each specimen. Each sample was acquired at a rate of approximately 5000 events per second. Quantification of miRNA-MB hybridization was measured by incubating at 37 °C the MB-beads with 50 nM of synthetic miRNA oligonucleotide target analog and reading the samples by flow cytometry at the indicated times (0, 1, 5, 10, 20, and 30 min of incubation). The specificity of the interaction was determined for different hsa-miR-451a mismatch analog sequences (WT, and mutations 1, 2, 3, and 4, see Table 1). Target and mutation analog sequences were incubated at 55 °C for 30 min before analysis.

2.6. miRNA-MB hybridization detection by gel electrophoresis

Different concentrations of MB (from 10 nM to 100 nM) were incubated with various concentrations of synthetic miRNAs or DNA

Table 1
Molecular beacons and target sequences.

miRNAs	Target sequences	MB sequences
hsa-miR-451a	rArArArCrCrGrUrUrArCrCrArUrUrArCrUrGrArGrUrU	5'-/56-FAM/CGC GAT C- AACTCAGTAATGGTAACGGTTT- G ATC GCG/ZEN//ISp18//3Bio/-3′
hsa-miR-451a mutation 1	rArArArCrCrGrUrUrArArCrArUrUrArCrUrGrArGrUrU	
hsa-miR-451a mutation 2	rArArArCrCrGrUrUrArArArArUrUrArCrUrGrArGrUrU	
hsa-miR-451a mutation 3	rArArArCrCrGrUrUrArArCrCrArUrUrArCrUrGrArGrUrC	
hsa-miR-451a mutation 4	rArArArCrCrGrUrUrArArCrCrArUrUrArCrUrGrArGrCrC	
hsa-miR-486-5p	rUrCrCrUrGrUrArCrUrGrArGrCrUrGrCrCrCrCrGrArG	5'-/56-FAM/CGC GAT C- CTCGGGGCAGCTCAGTACAGGA -G ATC GCG/ZEN//ISp18//3Bio/-3′
hsa-miR-16-5p	rUrArGrCrArGrCrArCrGrUrArArArUrArUrUrGrGrCrG	5'-/56-FAM/CGC GAT C- CGCCAATATTTACGTGCTGCTA-G ATC GCG/ZEN//ISp18//3Bio/-3′
hsa-miR-92a-3p	rUrArUrUrGrCrArCrUrUrGrUrCrCrCrGrGrCrCrUrGrU	5'-/56-FAM/CGC GAT C- ACAGGCCGGGACAAGTGCAATA -G ATC GCG/ZEN//ISp18//3Bio/-3′
	Target sequences (DNA backbone)	
hsa-miR-451a	AAACCGTTACCATTACTGAGTT	

oligonucleotide target analogs (from 0.1 nM to 100 nM) for 30 min at 37 or 55 °C, as noted in figure legends. After incubation, the hybridized duplexes were mixed with Gel Loading dye (6×), and then loaded on Novex TBE 4–20% gels. Gel electrophoresis was performed with constant voltage for 10 min at 100 V, and then the voltage was increased to 150 V for an additional 40 min. The MB fluorescence signal was visualized using 6-Fluorescein or Alexa 488 channel on a ChemiDoc MP Imaging System (Bio-Rad, Hercules, CA). Exposure times were set on "Manual" and varied depending on the sample between 10 and 300 s. The gel electrophoresis kinetic assay was performed by incubating 10 nM MB with 10 nM of synthetic DNA oligonucleotide target analog at various time points (15 s, 1, 5, 10, 20, and 30 min). The samples were prepared in a final volume of 20 uL using a 96-well plate and kept at 37 °C. As all the time points had to be run simultaneously, DNA oligonucleotide target analog was added in a staggered order starting with the 30 min time point. After 10 min, the target was added to the 20 min time point well, and so forth. One-minute before the 30-minute incubation time expired, the 20 uL in each well were mixed with 4 uL of Gel Loading dye and loaded into the gel. For the "0 min" time point the beacon was mixed with the DNA oligonucleotide target analog, gel Loading dye, and then added directly into the gel. Once loaded, the samples were run at 95 V, constant voltage, for 1.5 h.

2.7. Blood draw, and RBC isolation

The current study was approved by the Beth Israel Deaconess Medical Center Institutional Review Board (IRB). Four milliliters of fresh whole blood were obtained via venipuncture using 5 mL of Vacutainer EDTA tubes (BD, Franklin Lakes, NJ) from five self-declared healthy volunteers. First, plasma was separated from whole blood by centrifugation of 500×*g* for 10 min. RBCs were isolated by diluting the whole blood 1:1 with HBSS, and passing the blood through an Acrodisc white blood cells (WBC) removal syringe filter (Pall Corporation, NY). RBCs were then washed in 1 mL of HBSS three times at 500×*g* for 10 min each, to remove any residual platelets.

2.8. RNA isolation, cDNA synthesis and qPCR

RBCs were collected from five self-declared healthy donors as described above. RBC small RNA was purified using miRNeasy Mini Kit (Qiagen) following manufacturer's protocol. Isolated RNA was quantified using Qubit™ microRNA Assay Kit in a Qubit 4 Fluorometer (Thermo Fisher). Gel bands were cut using a scalpel, and RNA was eluted from gel using MinElute Gel extraction kit (Qiagen). Complementary DNA (cDNA) synthesis was performed using TaqMan Advanced miRNA cDNA Synthesis Kit (Thermo Fisher). Quantitative PCR (qPCR) was performed using TaqMan Fast Advanced Master Mix (Thermo Fisher) in triplicates with the primers hsa-miR451a (ID 001105), hsa-miR486-5p (ID 478128_mir), hsa-miR-92a-3p (ID 000431), and hsa-miR16-5p (ID 000391) in a 7500 Fast Real-time PCR System (Applied Biosystems, US). The qPCR thermal cycling conditions were set as follow: Step 1: Enzyme activation at 95 °C for 20 s, 1 cycle; Step 2: Denaturing at 95 °C for 3 s, and anneal/extend at 60 °C for 30 s, 40 cycles. Analyses of the data (Ct values for each replicate) were performed using the standard curve method, and the threshold baseline was adjusted to 1.7 for all samples.

2.9. Gel imaging analysis

Gel electrophoresis TIFF images were uploaded in ImageJ software (National Institutes of Health, Bethesda, Maryland) and transformed into 8-bit images. Rectangles were draw to determine the region of interest comprising the area of the hybridized MB-miRNA positive bands, and gel lanes were plotted using the following tools: Select Analyze > Gels > Plot Lanes. A straight-line tool was used to close the peak of the respective bands, and the wand (tracing) tool was used to determine the area under the curve (AUC) of the peaks. No correction was applied in the gel images to measure the AUC.

2.10. Statistical analysis of the data

For the kinetic assay using fluorometry, the curve fitting was adjusted for non-linear regression using the following four parameters: bottom, top, logEC50 and Hillslope. For the dose -dependent fluorometric assays, linear regression and R-squared values (r^2) were used to test linearity between increasing concentrations of MB-target and detected fluorescence. The differences in MB fluorescence among WT and mutated sequences (M1 to M4) were analyzed by One-way Anova, and Dunnett's multiple comparison test. One asterisk represents $p \leq 0.05$, $^{**}p \leq 0.01$, $^{***}p \leq 0.001$, $^{****}p \leq 0.0001$. AUC from gel bands was measured using ImageJ software.

3. Results

3.1. Limitations of the fluorometry based MB hybridization readout

We designed and tested four MBs (miR451aMB, miR486-5pMB, miR92a-3pMB, and miR16-5pMB) to detect mature human miRNAs enriched in red blood cells (RBCs), and plasma (hsa-miR451a, hsa-miR486-5p, hsa-miR92a-3p, and hsa-miR-16-5p). The MBs hairpin conformations are shown in Fig. 1A. At 55 °C, the MB show different loop structures, due to their unique target miRNAs complementary sequence (Fig. 1A). We chose 55 °C based on previous reports (Bonnet

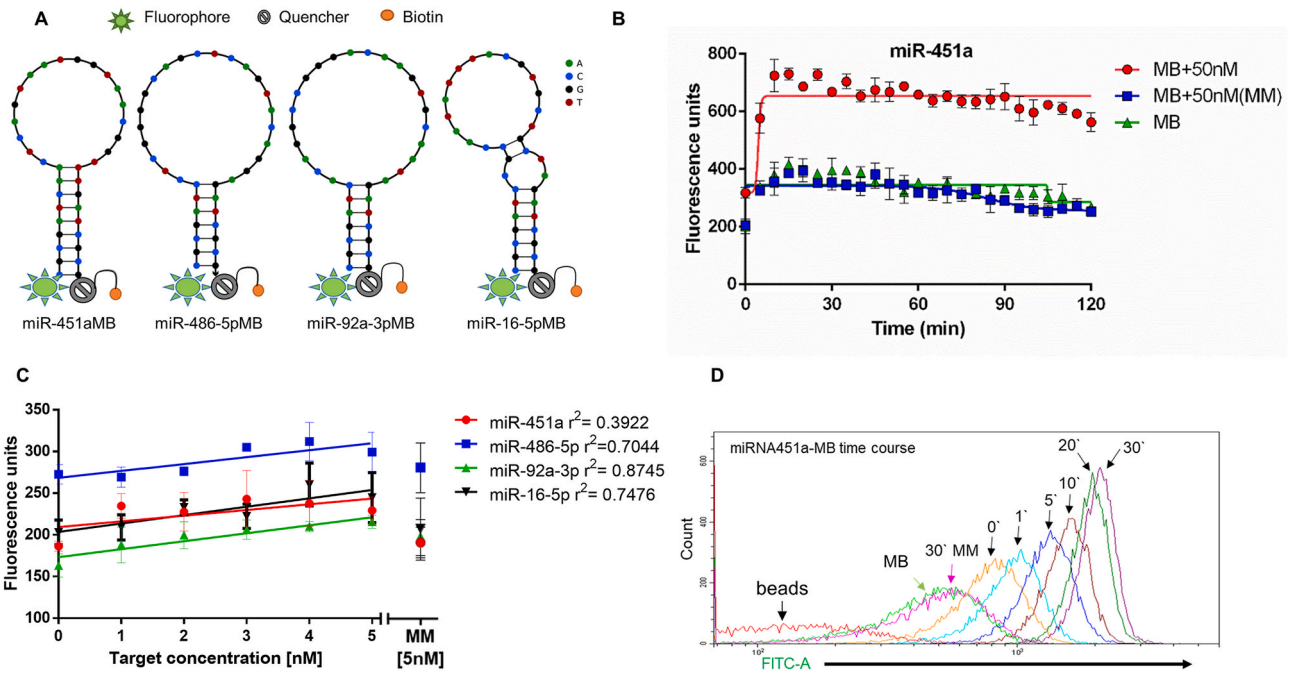

Fig. 1. Fluorometry and flow cytometry-based quantification of MB-miRNAs target analog hybridization. (A) Secondary conformation of the four MBs used (miR451aMB, 486-5pMB, 92a-3pMB, 16-5pMB) at 55 °C. Each MB is composed of a 5′-end 6-FAM, a CGCGATC stem sequence, a loop sequence complementary to its miRNA target, a 3′-end internal quencher, linker and a biotin molecule. (B) Kinetic fluorescence measurements (every 5 min for 2 h) generated by the MB alone (green line), MB-target (red line), and mismatched-target (blue line) hybridization. Lines were fitted using a nonlinear regression model. The fluorescence reached a peak between 20 and 30 min of incubation at 55 °C. (C) Dose dependence fluorescence values of the MB-miRNAs target analog from 1 to 5 nM, for 30 min at 55 °C. Lines were fitted using a linear regression of MB-miRNAs target analogs hybridization showing the respective r^2 values (D) Flow cytometric kinetic measurements of the 500 nm bead-attached MB following incubation with 50 nM of either mismatched miRNA (light purple histogram), or target miRNA measured at 0 (orange), 1 (light blue), 5 (cobalt blue), 10 (brown), 20 (green), or 30 (dark purple) min. For time 0, there was a delay of about 10–15 s between adding the miRNA to the MB-beads, mixing and actual acquisition of the data. The *X*-axis represents the intensity of fluorescence emitted by the MB following interaction with the miRNA. Data represent three independent experiments. Error bars indicate the s.e.m.*

et al., 1999) showing increased sensitivity on the MB for the target sequences than at 21 °C. *In silico* melting curve analysis showed similar MB melting temperatures (Supplementary Figure S1A). Next, we measured the fluorescence generated by the hybridization of MBs with 50 nM miRNAs target analogs or controls every 5 min for 2 h. The fluorescence peak was achieved between 20 and 30 min for all four MBs tested. The fluorescence background values were higher for miR451aMB (360–380 fluorescence units (FU)) with 2-fold increase over background (Fig. 1B). The other species, miR486-5pMB, miR92a-3pMB, and miR16-5pMB showed approximately 200 FU as a background, and 4.5, 3.5, and 5.6 fold increase over background, respectively (Supplementary Figure S1B). The effect of background fluorescence on the detection sensitivity becomes more apparent at low concentrations (1–5 nM) of the miRNAs target analogs, where the linearity of the signal (r^2) drops to 0.874 for miR92a-3pMB and 0.392 for miR451aMB (Fig. 1C). The low r^2 value for miR451aMB is not surprising as the background fluorescence of this MB had the highest value of the MB tested. The high background fluorescence seen in the MBs, could be explained either by the incomplete quenching of the fluorochrome by the quencher, random coil configurations of the MBs, which further lowers the efficiency of quenching, or the presence of free dye in the MB solution. To test for the presence of free dye, we coupled MBs to streptavidin beads, and after washing the beads, we added the miRNAs target analogs and measured the fluorescence over time (5 s, 1, 2, 5, 10, 20, and 30 min) by flow cytometry. The results from flow cytometry showed the presence of higher background fluorescence in the MB conjugated with beads compared to the beads alone. This result suggests that the MB background fluorescence was not due to the presence of free dye in MB solution but mostly from incomplete quenching or random coil configurations (Fig. 1D).

3.2. Hybridization of the molecular beacon to the target alters its electrophoretic properties

Based on the fluorometry results, we next tested whether gel electrophoresis would provide an alternative detection means, while at the same time reducing MB fluorescence background thus improving sensitivity. The principle of MB-based nucleic acid detection using gel electrophoresis, relies on orthogonal conformation of the MB binding to the target: i) slower electrophoretic mobility on the MB hybridized with its target compared to the MB alone, and ii) a dose dependent fluorescence of the MB upon hybridization with target. We began by testing the sensitivity of the method by incubating 100 nM of miR451aMB with increasing concentrations of miRNAs target analogs (0, 1, 50, and 100 nM). The fluorescent band intensity representative of the MB-target hybridization (higher band, arrow) increased, as expected in a dose-dependent manner. Simultaneously, the gel also showed a progressive decrease in the fluorescence pattern of the unbound MB (lower bands), showing the depletion of the MBs paralleling the increase of the target (Fig. 2A, Supplementary Figure S2A). Next, we test increasing concentrations of target (1–5 nM) using four different MBs. The results show that each MB has a specific electrophoretic mobility pattern, with miR451aMB showing lowest separation between bound and unbound hybridization products, while miR486-5pMB showed highest separation. All four MB tested showed a positive signal using 1 nM of target (Fig. 2B). We also detected a pattern of some of the faster fluorescent bands bellow the positive signal of MB-target duplex. These fastest bands were only visible when low concentration of targets and longer exposures times were used. When area under the curve (AUC) for the positive gel bands was measured (1–5 nM), all MB showed a strong linearity with r^2 above 0.98 (Fig. 2C). We also tested sub-nanomolar

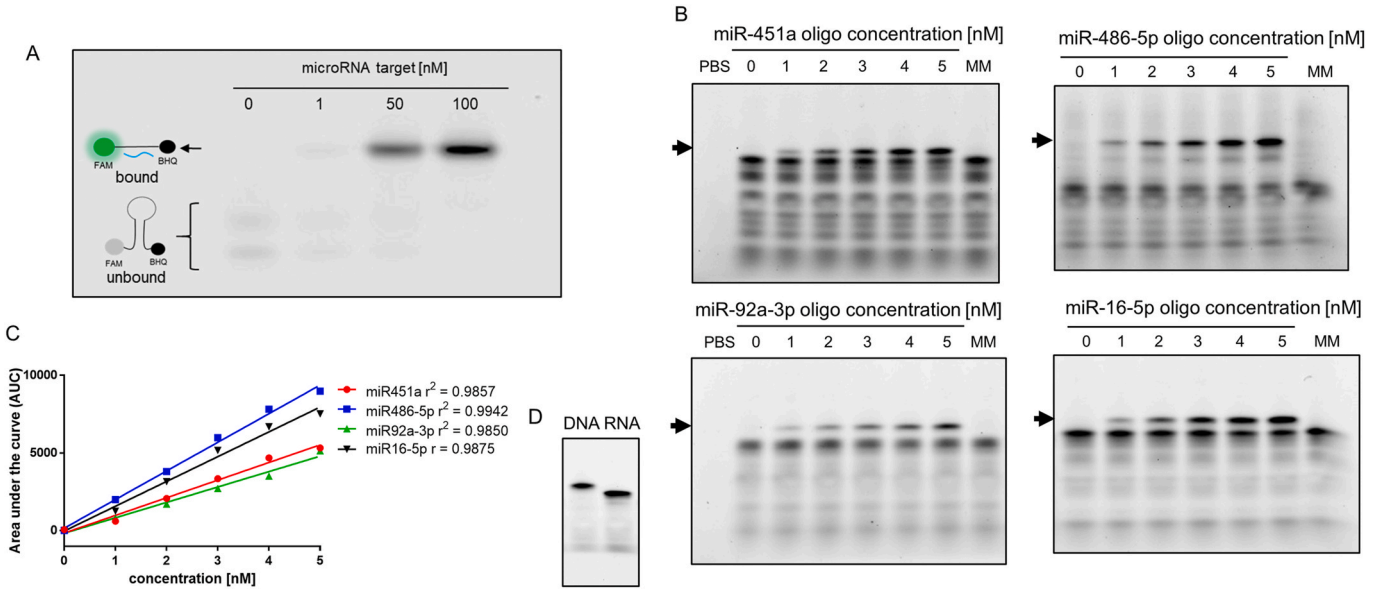

Fig. 2. Electrophoretic mobility patterns of unbound and bound molecular beacons (MB). (A) miR451aMB (100 nM) was hybridized with increasing concentration of hsa-miR-451a target analogs (0, 1, 50, and 100 nM), followed by gel electrophoresis. Top band represents the duplex MB-target hybridization (lower electrophoretic mobility), while bottom bands represent unbound MB (higher electrophoretic mobility) (B) MBs (50 nM) were incubated with increasing concentrations of corresponding miRNA target analogs (0–5 nM). The pattern of top (duplex MB-target analog), and bottom (unbound MB) bands was maintained. (C) Linear regression was calculated using area under the curve (AUC) values measured from positive fluorescence bands MB-miRNA target analog (top bands). (D) miR451aMB (50 nM) was incubated with same concentration (50 nM) of either a DNA backbone hsa-miR451a or RNA backbone hsa-miR451a.

concentrations of the target analogs (100–500 pM). We were able to detect a band with 100 pM for certain miRNA depending on the sequence tested (Supplementary Figure S2B). Using the same concentrations (100–500 pM) of targets, fluorometry showed a weak linearity with r^2 between 0.07 and 0.28 (Supplementary Figure S2C), while r^2 values obtained from gel electrophoresis positive bands (AUC) were between 0.67 and 0.82. (Supplementary Figure S2D). We compared the MB electrophoretic mobility using DNA or RNA backbone as target analogs, as this approach is not limited to RNA detection. The results in Fig. 2D, show that RNA backbone has higher electrophoretic mobility than the corresponding DNA analog, likely due to the difference in charge between the two backbones. We next performed a kinetic experiment by incubating 50 nM MBs for increasing amounts of time, 15 s, 1, 5, 10, 20, or 30 min, with 50 nM of the target analog at 37 °C. The results (Supplementary Figure S3A) showed that the signal is visible even when the co-incubation time is approximately 15 s, reaching a fluorescence peak in 20 min, after which the signal plateaus. These results are consistent with the fluorometry (Fig. 1B), and flow cytometry data (Fig. 1D). To further understand if the downstream fluorescent bands were a result of impure MBs due to synthesis and/or storage, we performed gel electrophoresis in the presence of 7M Urea (denaturing conditions). Our results show that the opened MBs generated a strong fluorescent top band with several faster bands still present, although with significant decreased fluorescence (Supplementary Figure S3B). The fastest bands were likely due to autofluorescence of the loading buffer, as there are also seen in PBS plus loading buffer lane. The remaining bands, could be due to fluorochrome-bearing oligonucleotide fragments, incomplete reduction of the beacons by urea (unlikely due to the high concertation used, 7M), or through and yet to be described mechanism (Ryazantsev et al., 2014).

3.3. Electrophoretic mobility can identify hybridization of MB to mutated miRNA target analogs

Current molecular beacon-based methods for detection of point mutation afford identification of single mutation as long as the mismatched nucleotide is flanked on either side by at least one functional base pair (Bonnet et al., 1999). We tested the ability of the electrophoretic mobility shift to differentiate between the wild type miRNA target analog and several 1 and 2 nt mutated miRNA target analog sequences (Table 1). Analyses of the MB hybridization with WT or mutated sequences performed by Nupack software (available at http://www.nupack.org/) indicated the presence of a mismatched loop in the middle of the duplex MB-target analog sequence when MB was incubated with mutated sequences 1 (M1), and 2 (M2) (Fig. 3A). We compared the ability of fluorometry, flow cytometry and electrophoretic mobility shift to detect differences in the hybridization of the MB-WT, or MB-Mutated sequences. For this comparison, miR451aMB was conjugated with 500 nm streptavidin beads (Supplementary Figure S4A), followed by incubation with either 50 nM of WT or mutated miR451a target analog sequences (M1 to M4).

The cumulative results of four independent experiments showed that of all the mutations, fluorometry was only able to distinguish between WT and M2 sequence (center, CC to AA, $p = 0.0165$) (Fig. 3B). Flow cytometry analysis correctly identified center mutations, M1 (center, C to A, $p < 0.0001$), as well as M2 (center, CC to AA, $p < 0.0001$). There was no statistical difference between WT and the 5′-end mutation M3 (5′-end, U to C, ns $p = 0.9998$), while in the case of M4 mutation (5′-end, AA to CC) there was a significant ($p = 0.0019$) decrease in the fluorescence signal. (Fig. 3C, and D). The electrophoresis approach correctly identified the center mutations, with M1 (center, C to A, $p < 0.0001$) showing a dimmer band, and M2 mutation (center, CC to AA, $p < 0.0001$) generating virtually no band. Similarly to flow cytometry, gel electrophoresis could not identify the single end mutation, M3 (5′-end, U to C, ns $p = 0.0847$), but it correctly identified the double end mutation M4 (5′-end, AA to CC, $p < 0.0001$) by both fluorescence intensity as well as electrophoretic mobility, showing a slightly higher band, which was more pronounced in the case of DNA backbone compared to RNA (Fig. 3E and F, and Supplementary Figure S4B).

Thus, our results showed that flow cytometry and electrophoretic mobility detection performed better than fluorometry in detecting mutations in miRNA target sequences.

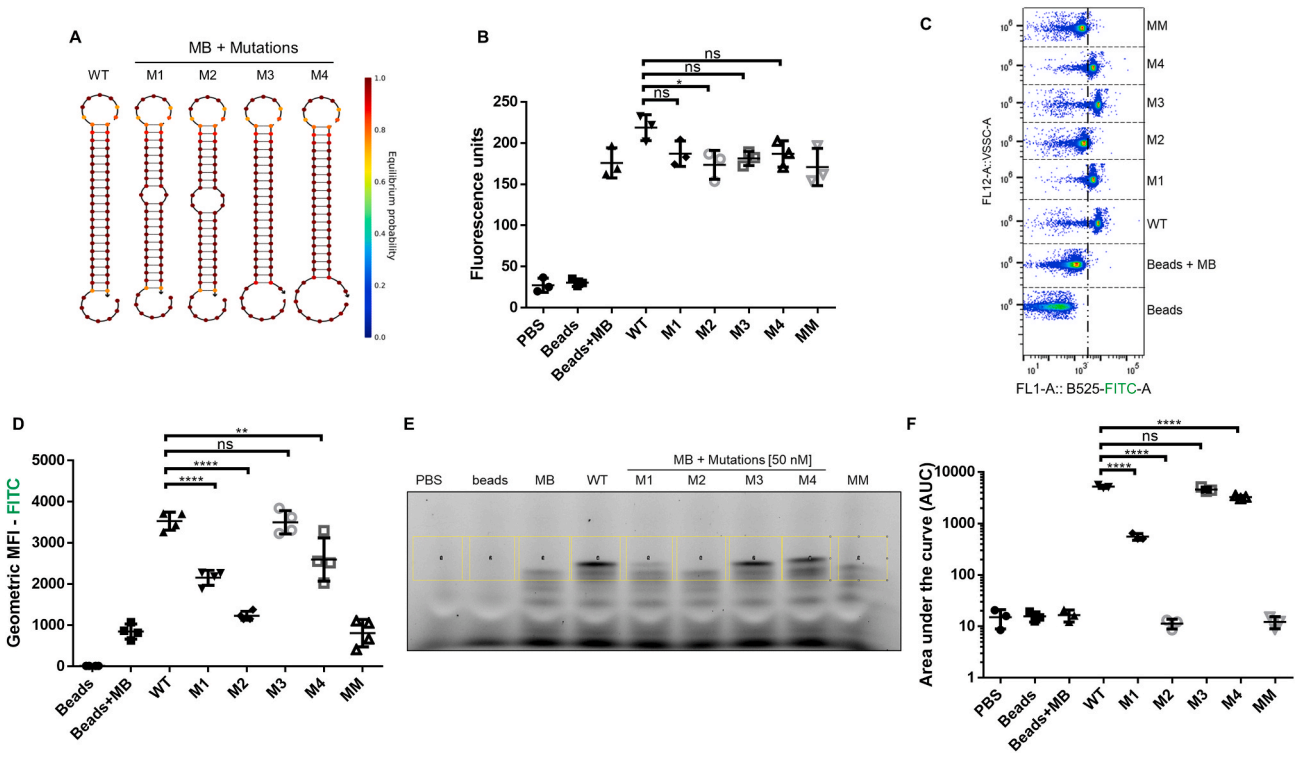

Fig. 3. Electrophoretic mobility shift differentiates certain hsa-miR-451a mutated sequences. (A) Secondary structures of different hybridization patterns between miR451aMB hybridized with WT or hsa-miR-451a mutated sequences M1 (center C to A), M2 (center CC to AA), M3 (5′-end U to C), and M4 (5′-end UU to CC). Heat map represents the minimum free energy between the hybridization of each base pair. (B) One-hundred nM of miR451a MB were coupled with 500 nm streptavidin beads and hybridized with 50 nM of hsa-miR451a WT or mutated sequences (M1 to M4). Fluorescence was measured by fluorometry after 30 min incubation at 55 °C. (C) Flow cytometric analysis of MB-beads incubated with 50 nM of either miR451a (WT), various mutations of miR451a (M1-M4), or MM (miR486). X-axis shows fluorescence intensity of the FAM MB fluorochrome, and Y-axis represent violet side scatter values of the 500 nm beads (D) Flow cytometry geometric mean fluorescence intensity analysis of miR451aMB hybridized with hsa-miR-451a WT or mutated sequences M1 to M4 (E) Gel electrophoresis of the miR451aMB hybridized with hsa-miR-451a WT or mutated sequences M1 to M4. Yellow squares represents the region of interest for measuring the area under the curve (AUC). (F) AUC of miR451aMB hybridized with WT or mutated sequences. Data represent three to four independent experiments. Error bars indicate the s.e.m. One-way Anova, and Dunnett's multiple comparison test were performed. One asterisk represents $p \leq 0.05$, **$p \leq 0.01$, ***$p \leq 0.001$, ****$p \leq 0.0001$.

3.4. Electrophoretic mobility shift can identify endogenous miRNA species

We next sought to validate the approach using purified RNA from blood cells, specifically red blood cells (RBCs). Total RNA from RBCs was isolated from five self-declared healthy donors and the levels of hsa-miR-451a were measured using both RT-qPCR and gel electrophoresis. For the electrophoretic mobility assay, we incubated 100 nM of miR451aMB with increasing amounts (25, 75, 150, and 250 ng) of total RBCs purified RNA. As a positive and negative confirmation of the bands, we used hsa-miR-451a, and hsa-miR-486-5p miRNA target inhibitors. Similar to the results obtained using synthesized RBC miRNAs, the fluorescence intensity of the miR451aMB-target band increased with the amount of RBC RNA added to the reaction. The positive band did not form when the RNA was pre-incubated with hsa-miR-451a miRCury LNA Inhibitors (anti-miRs). The MB-miR451a hybridization was not affected when incubating the RNA with a hsa-miR-486-5p inhibitor, further confirming the identity of the positive band as the presence of a duplex MB-hsa-miR-451a (Fig. 4A). To further confirm the identity of the MB-miRNAs duplex, we cut two fluorescent negative gel bands (control samples), one in the miR451aMB lane, and a second one in the miR451aMB-miR-451a Inhibitors, as well as the fluorescently positive bands obtained from the hybridization of miR451aMB (Fig. 4B, highlighted in red). The gel fragments were then eluted, the RNA was isolated, and qPCR was performed to detect four highly present miRNAs in RBC and plasma: hsa-miR451a, 486-5p, 92a-3p, and 16-5p. Quantitative PCR results indicate that areas with positive fluorescence bands corresponding to the putative miR451aMB-RNA target complex showed the lowest Ct values for hsa-miR-451a, as compared to the others miRNAs from all five donors (Fig. 4C). None of the miRNAs were detected in the negative control bands (miR451aMB alone). Furthermore, the Ct values from hsa-miR-451a increased from 22 to 29 when incubating the RNA previously with hsa-miR-451a inhibitor (Supplementary Figure S5).

4. Discussion

For several decades, fluorometry was the standard method used to quantify the fluorescence triggered by the binding of MB to their target sequences (Tyagi and Kramer, 1996). This method affords, unlike cell-based approaches, a tight control over experimental conditions such as MB and target concentration, buffer pH and composition, ion content, as well as changes in temperature during experiments. Furthermore this method allows MB fluorophore multiplexing (Marras et al., 1999; Zhang et al., 2001), conjugation of MB with gold nanoparticles (Mao et al., 2009) or qDots (Mahani et al., 2019). In addition to the stable and controlled conditions, the frequency of sample interrogation can be set anywhere between seconds to tens of minutes. A drawback of fluorometry is bulk reading of the reaction solution when the presence of free fluorophore, incomplete quenching, and degraded beacon will significantly increase the noise, and decrease the sensitivity.

Herein, we describe a gel electrophoresis-based readout method to detect specific miRNAs in the picomolar range. We have previously reported the use of nanoswitches for detecting specific proteins in suspension (Hansen et al., 2017), and this work has been extended by others to detect miRNA (Chandrasekaran et al., 2019). DNA nanoswitches are self-assembled nanoscale devices that undergo a conformational change in response to a specific binding event (Koussa et al.,

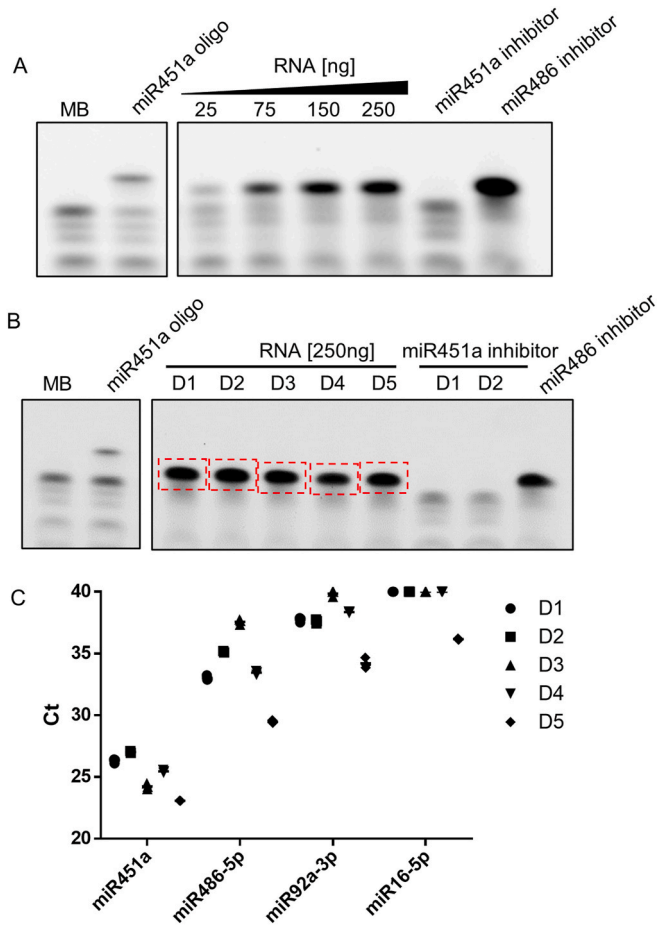

Fig. 4. Identification of endogenous hsa-miR-451a by MB hybridization and electrophoretic mobility shift. (A) Detection of hsa-miR-451a in increasing concentrations of total RNA purified from RBCs isolated from a donor. The miR451a signal did not form when the isolated total RNA was preincubated with miR451a inhibitor. (B) Two hundred fifty nanograms of total RNA RBCs isolated from five self-declared healthy donors (D1 to D5) were incubated with miR451aMB. The MB-miRNAs hybrid bands (red rectangles) were cut, and the eluted RNA was prepared for qPCR. (C) Confirmation of the identity of the target in MB-miRNAs bands. Quantitative PCR data obtained from five donors shows the lowest Ct values for miR451a, followed by miR-16-5p. miR92a was not identified in any of the samples, and the sample were represented by Ct of 40.

2015). Unlike the nanoswitch method, the approach presented here uses off-the-shelf MB, bypassing the need for synthesis and coupling protocols. The built-in on/off fluorescence reporter generates light only when the MB is hybridized with the intended target (Tyagi and Kramer, 1996), circumventing the need for additional staining steps, and due to the delayed electrophoretic mobility of the MB-target duplex, the location of the positive fluorescent band also acts as an orthogonal confirmation of the specificity of target binding.

During gel electrophoresis, we noticed several fluorescent bands bellow the positive bands representative of the hybridization between MB and miRNA target analogs. These faster bands were more visible when we used low concentration of targets (0.1–0.5 nM, and 1–5 nM, Fig. 2B, and Supplementary Figure S2B) and long exposure times (180 s). However, when we used high concentrations of targets (above 10 nM, Fig. 2A, Supplementary Figure S2A) and low exposure times (1–5 s), the faster bands were almost invisible. The faster bands could be generated by incomplete quenching of the fluorochrome, which means that the MB may have a hairpin structure with a small fraction of fluorophore which is still not effectively quenched upon excitation (incomplete Förster resonance) or an alternating configurations between hairpin to random coil (Ryazantsev et al., 2014), which will also have different migration patterns. This last explanation seems likely as certain bands below the MB-miRNA hybrid fade away and then disappear as the concentration of the target increases (Fig. 2A, Supplementary Figure S2A). Moreover, in Supplementary Figure S3B, we have run a denaturing gel to further address this issue. As all the MBs were in the linear conformation during electrophoresis regardless of the presence of the target miRNAs, the additional bands seen on the gel (less than 5–10%), could be due to: i) fragments of the MB, ii) incomplete reduction of the beacons by urea due to strong secondary structures which can still remain intact even under denaturing conditions, or through and yet unknown mechanism (Ryazantsev et al., 2014).

The sensitivity limit of this approach depends primarily on the brightness of the fluorochromes, the sensitivity of the imaging device, and the autofluorescence of agarose or polyacrylamide gels. We report here a detectable band of 100pM for all four MB tested. Quantum dots (qDots) have been used successfully as MB fluorochromes for increasing the sensitivity of the signal, and affording longer integration times with limited photo bleaching (Adegoke and Park, 2017; Mahani et al., 2019). As the size of qDots is between 10 and 20 nm (Murray et al., 2000) we do not expect this approach to hinder the migration of the MB or MB-target complex on the gel.

During gel electrophoresis, the relative mobility of migrating molecules depends on their size, conformation, and when running the samples in SDS-free conditions, their overall charge (Gallagher, 2012). We found (Fig. 2D) that the difference in the relative electrophoretic mobility between MB and DNA or RNA backbone target analogs is likely due to the presence of an additional hydroxyl residue on C2 of ribose compared to deoxyribose.

When we investigated the ability of gel electrophoresis to identify several mutations in the miRNA sequence (Fig. 3), we found that the location and number of the mismatched nucleotides in the electrophoretic pattern of the duplex miR451aMB-WT or miR451aMB-mutated sequences was critical for understanding the gel profile. Our data is consistent with previous reports showing only partial loss in fluorescence signal for single nucleotide mutation mismatch in target sequences (Dubertret et al., 2001; Mahani et al., 2019; Qiu et al., 2013). Obtaining a binary answer regarding the presence of a point mutation in the target sequence flanked by non-mutated nucleotides, requires a more elaborate approach involving the measurement of thermal denaturation profiles of the MB-targets, followed by identification of the gap between the transition temperatures of matched and point-mutated duplexes. Once the two temperatures are known, the readout is performed within the temperature range where the matched duplex is still fluorescent, and the single nucleotide mismatched target is no longer hybridized to the MB(Bonnet et al., 1999). Therefore, for detection of certain mutations (M2 and M4) gel electrophoresis has advantages over flow cytometry, while for others (M1 and M3) offers no benefits. While flow cytometry requires conjugation of MB to beads, expensive flow cytometry equipment, and trained personnel, gel electrophoresis provides orthogonal, quantitative confirmation of the MB-target binding in a fast and affordable way. The approach described here could be multiplexed for detection of several nucleic acid targets in the same lane using MBs conjugated to various fluorochromes (Marras et al., 1999).

The gel electrophoresis-based readout is fully applicable to identifying various ssRNA and ssDNA molecules found in biological fluids, such as, viruses, circulating RNA complexes, cell-free DNA, and nucleic acids associated with extracellular vesicles (Fuchs et al., 2000). In Fig. 4, we show that electrophoretic mobility method described here can be used to detect a miRNA enriched in RBCs and plasma, opening possibilities for the use of this approach in detecting specific DNA or RNA sequences in various biofluids (liquid biopsies), as well as solid tissues. As certain sequences of interest may not be readily available for MB hybridization due to either secondary structure, or the presence of interacting proteins, incubating the sample with helper oligos, which flank the target site, may also improve the chances for a positive MB

signal (Bhadra and Ellington, 2014). For double-stranded nucleic acids, using the direct MB approach as described here is not feasible, unless the selected region is present in a loop of the molecule where the beacon has access (Baker et al., 2012), or when using a CRISPR/cas9-MB tandem approach, as was recently reported in living cells (Wu et al., 2018b). For transcripts longer than miRNAs, using several MB and FRET MB tandems would also lower the detection limit and provide an opportunity for multiplexing, as well as testing for insertions/deletions/mutations in given sequences (Chen et al., 2017). However, longer RNA molecules, as is common in mRNA molecules or certain viruses, may require mechanical sheering or enzymatic cleavage prior to gel detection to allow effective gel penetration of the genetic material.

5. Conclusions

Electrophoretic mobility shift assay allows specific and sensitive detection of RNA and DNA molecules in biologically relevant samples. The chief advantage of this method is based on its orthogonal confirmation of the binding event and identify of the target, by a shift in the electrophoretic mobility and gain in fluorescence of the MB-target duplex. In addition, the electrophoretic mobility approach is impervious to the MB fluorescence caused by free fluorophores and incomplete quenching present in the solution, further increasing the sensitivity of the method. As a biosensor technology, our method can be scalable to be used in a single-probe strip test for the rapid and sensitive multiplex detection of small RNA or DNA sequences, as reported previously for miR-21 detection using MB (Kor et al., 2016).

Credit author statement

GPOJ, Conceptualization, Methodology, Formal analysis, Investigation, Data curation, Writing – original draft, Writing – review & editing, Visualization. WPW, Conceptualization, Resources, Supervision, Project administration, Funding acquisition. ICG, Conceptualization, Formal analysis, Resources, Data curation, Writing – original draft, Writing – review & editing, Supervision, Project administration, Funding acquisition. RHB, Methodology, Validation, Investigation, Visualization. LT, Methodology, Validation, Investigation, Visualization. BP, Methodology, Validation, Investigation. MMT, Methodology, Validation, Investigation. SL, Methodology, Investigation, Data curation. CHH, Methodology, Resources, Writing – review & editing. JT, Methodology, Formal analysis, Writing – review & editing, Supervision. JJ, Resources, Writing – review & editing, Project administration, Funding acquisition.

Funding

This work was supported by the following National Institutes of Health grants to ICG: RO1CA218500, UG3HL147353, and UG3TR002881, and NIGMS R35 GM119537 to WW.

Declaration of competing interest

The authors declare the following financial interests/personal relationships which may be considered as potential competing interests: Beth Israel Deaconess Medical Center (GPO, ICG), and Boston Children's Hospital (WPW) have submitted a patent covering the methods described in this manuscript. The other co-authors declare no conflict of interest.

Acknowledgements

We would like to thank Professor Sanjay Tyagi (Rutgers University) for useful technical discussions regarding molecular beacons, and Dr. Glenn Merrill-Skoloff (BIDMC) for help with gel imaging.

Appendix A. Supplementary data

Supplementary data to this article can be found online at https://doi.org/10.1016/j.bios.2021.113307.

References

Adegoke, O., Park, E.Y., 2017. J. Mater. Chem. B 5 (16), 3047–3058.
Baker, M.B., Bao, G., Searles, C.D., 2012. Nucleic Acids Res. 40 (2), e13.
Bhadra, S., Ellington, A.D., 2014. RNA 20 (8), 1183–1194.
Bonnet, G., Tyagi, S., Libchaber, A., Kramer, F.R., 1999. Proc. Natl. Acad. Sci. Unit. States Am. 96 (11), 6171–6176.
Burris, K.P., Wu, T.-C., Vasudev, M., Stroscio, M.A., Millwood, R.J., Stewart, C.N., 2013. IEEE Trans. NanoBioscience 12 (3), 233–238.
Bushati, N., Cohen, S.M., 2007. Annu. Rev. Cell Dev. Biol. 23, 175–205.
Camacho, V., Toxavidis, V., Tigges, J.C., 2017. Extracellular Vesicles. Springer, pp. 175–190.
Chandrasekaran, A.R., MacIsaac, M., Dey, P., Levchenko, O., Zhou, L., Andres, M., Dey, B.K., Halvorsen, K., 2019. Sci. Adv. 5 (3), eaau9443.
Chen, M., Ma, Z., Wu, X., Mao, S., Yang, Y., Tan, J., Krueger, C.J., Chen, A.K., 2017. Sci. Rep. 7 (1), 1–11.
Choi, Y.S., Edwards, L.O., DiBello, A., Jose, A.M., 2017. Nucleic Acids Res. 45 (10), e87.
de Oliveira Jr., G.P., Zigon, E., Rogers, G., Davodian, D., Lu, S., Jovanovic-Talisman, T., Jones, J., Tigges, J., Tyagi, S., Ghiran, I.C., 2020. iScience 23 (1), 100782.
Dubertret, B., Calame, M., Libchaber, A.J., 2001. Nat. Biotechnol. 19 (4), 365–370.
Fuchs, B.M., Glöckner, F.O., Wulf, J., Amann, R., 2000. Appl. Environ. Microbiol. 66 (8), 3603–3607.
Gallagher, S.R., 2012. Curr. Protoc. Mol. Biol. 97 (1), 10.12.A.11–10.12.A.44.
Hansen, C.H., Yang, D., Koussa, M.A., Wong, W.P., 2017. Proc. Natl. Acad. Sci. Unit. States Am. 114 (39), 10367–10372.
Hatfield, S., Shcherbata, H., Fischer, K., Nakahara, K., Carthew, R., Ruohola-Baker, H., 2005. Nature 435 (7044), 974–978.
Horejsh, D., Martini, F., Poccia, F., Ippolito, G., Di Caro, A., Capobianchi, M.R., 2005. Nucleic Acids Res. 33 (2), e13.
Izzotti, A., Carozzo, S., Pulliero, A., Zhabayeva, D., Ravetti, J.L., Bersimbaev, R., 2016. Am. J. Cancer Res. 6 (7), 1461.
James, A.M., Baker, M.B., Bao, G., Searles, C.D., 2017. Theranostics 7 (3), 634.
Kam, Y., Rubinstein, A., Nissan, A., Halle, D., Yavin, E., 2012. Mol. Pharm. 9 (3), 685–693.
Kor, K., Turner, A.P., Zarei, K., Atabati, M., Beni, V., Mak, W.C., 2016. Anal. Bioanal. Chem. 408 (5), 1475–1485.
Koussa, M.A., Halvorsen, K., Ward, A., Wong, W.P., 2015. Nat. Methods 12 (2), 123–126.
Kozomara, A., Birgaoanu, M., Griffiths-Jones, S., 2019. Nucleic Acids Res. 47 (D1), D155–D162.
Lee, R.C., Feinbaum, R.L., Ambros, V., 1993. Cell 75 (5), 843–854.
Li, Y.-Q., Guan, L.-Y., Wang, J.-H., Zhang, H.-L., Chen, J., Lin, S., Chen, W., Zhao, Y.-D., 2011. Biosens. Bioelectron. 26 (5), 2317–2322.
Li, Y., Jiang, J., Liu, W., Wang, H., Zhao, L., Liu, S., Li, P., Zhang, S., Sun, C., Wu, Y., 2018. Proc. Natl. Acad. Sci. Unit. States Am. 115 (46), E10849–E10858.
Mahani, M., Mousapour, Z., Divsar, F., Nomani, A., Ju, H., 2019. Microchim. Acta 186 (3), 132.
Mao, X., Xu, H., Zeng, Q., Zeng, L., Liu, G., 2009. Chem. Commun. (21), 3065–3067.
Marras, S.A., Kramer, F.R., Tyagi, S., 1999. Genet. Anal. Biomol. Eng. 14 (5–6), 151–156.
Mestdagh, P., Van Vlierberghe, P., De Weer, A., Muth, D., Westermann, F., Speleman, F., Vandesompele, J., 2009. Genome Biol. 10 (6), 1–10.
Murray, C.B., Kagan, a.C., Bawendi, M., 2000. Annu. Rev. Mater. Sci. 30 (1), 545–610.
Qiu, L., Wu, C., You, M., Han, D., Chen, T., Zhu, G., Jiang, J., Yu, R., Tan, W., 2013. J. Am. Chem. Soc. 135 (35), 12952–12955.
Ryazantsev, D.Y., Kvach, M.V., Tsybulsky, D.A., Prokhorenko, I.A., Stepanova, I.A., Martynenko, Y.V., Gontarev, S.V., Shmanai, V.V., Zavriev, S.K., Korshun, V.A., 2014. Analyst 139 (11), 2867–2872.
Sandbothe, M., Buurman, R., Reich, N., Greiwe, L., Vajen, B., Gürlevik, E., Schäffer, V., Eilers, M., Kühnel, F., Vaquero, A., 2017. J. Hepatol. 66 (5), 1012–1021.
Shi, H., Ji, Y., Zhang, D., Liu, Y., Fang, P., 2016. Oncol. Rep. 36 (5), 3051–3057.
Tan, W., Wang, K., Drake, T.J., 2004. Curr. Opin. Chem. Biol. 8 (5), 547–553.
Tyagi, S., Kramer, F.R., 1996. Nat. Biotechnol. 14 (3), 303–308.
Wu, R., Zeng, J., Yuan, J., Deng, X., Huang, Y., Chen, L., Zhang, P., Feng, H., Liu, Z., Wang, Z., 2018a. J. Clin. Invest. 128 (6), 2551–2568.
Wu, X., Mao, S., Yang, Y., Rushdi, M.N., Krueger, C.J., Chen, A.K., 2018b. Nucleic Acids Res. 46 (13), e80.
Zhang, K., Yang, X.-J., Zhang, T.-T., Li, X.-L., Chen, H.-Y., Xu, J.-J., 2019. Anal. Chim. Acta 1079, 146–152.
Zhang, P., Beck, T., Tan, W., 2001. Angew. Chem. 113 (2), 416–419.